Perturbation of the yield-stress rheology of polymer thin films by nonlinear shear ultrasound

J. Léopoldès
LPMDI, Université Paris-Est, 5 Boulevard Descartes, 77454 Marne-la-Vallée Cedex 2, France

G. Conrad
LPMDI, Université Paris-Est, 5 Boulevard Descartes, 77454 Marne-la-Vallée Cedex 2, France

X. Jia
Institut Langevin, ESPCI ParisTech, CNRS UMR No. 7587, 1 Rue Jussieu, 75005 Paris, France and Université Paris-Est, 5 Boulevard Descartes, 77454 Marne-la-Vallée Cedex 2, France

(Received 9 October 2014; published 15 January 2015)

We investigate the nonlinear response of macromolecular thin films subjected to high-amplitude ultrasonic shear oscillation using a sphere-plane contact geometry. At a film thickness comparable to the radius of gyration, we observe the rheological properties intermediate between bulk and boundary nonlinear regimes. As the driving amplitude is increased, these films progressively exhibit oscillatory linear, microslip, and full slip regimes, which can be explained by the modified Coulomb friction law. At highest oscillation amplitudes, the interfacial adhesive failure takes place, being accompanied by a dewettinglike pattern. Moreover, the steady state sliding is investigated in thicker films with imposed shear stresses beyond the yield point. We find that applying high-amplitude shear ultrasound affects not only the yielding threshold but also the sliding velocity at a given shear load. A possible mechanism for the latter effect is discussed.

DOI: 10.1103/PhysRevE.91.012405 PACS number(s): 81.40.Pq, 43.35.+d, 62.20.Qp

I. INTRODUCTION

The transition from a static solid state to a sliding fluid state plays an essential role in a wide range of driven systems, including molecularly thin films, ferromagnets, contact lines of droplets, glasses, and seismic fault gouges [1–10]. Various rate- and state-dependent constitutive laws are developed to describe the threshold rheology at the wide range of length scales. For solid friction, molecularly thin lubricant films control the sliding dynamics of the interface. As the thickness h is decreased, both confinement effect and nonlinear response (e.g., stick-slip) may manifest. Highlighting the mechanisms responsible for the nonlinear rheology of thin films is essential for understanding phenomena such as dewetting and interfacial fracture [11,12].

Shear ultrasonic vibration provides a controlled oscillatory rheological measurement of thin films ($h \sim 1$–100 nm) over a large range of shear strain $\epsilon_T \sim U_T/h$, with $U_T \sim 0.1$–100 nm the amplitude of shear displacement) [10]. Previous ultrasonic measurements performed on thin films confined at a sphere-plane contact [13,14] showed that the interfacial rheology exhibits various characteristics between bulk and boundary lubrication regimes [15]. For the interface adsorbed with the thick film $h > 100$ nm, the interfacial oscillatory rheology is independent of shear driving U_T, indicative of a linear response over the available amplitude range. The response is basically controlled by the viscoelastic properties of the polymer layer bonded at the interface.

In the case of confined thin films $h \sim 1$ nm, the interfacial rheology is determined by the friction dynamics. When U_T is less than a critical value U_c, the whole contact area is stuck. The linear response is dominated by the viscoelastic properties of the solids in contact. When $U_T > U_c$, the periphery of the contact exhibits a solid-to-fluid transition via plastic deformation and the tangential vibrations induce the growth of a microslip annulus as described by the model of Mindlin [16]. The stuck part of the contact area decreases correspondingly when the oscillatory force reaches the Coulomb-like force threshold $F_s = F_{adh} + \mu N$, where F_{adh} is the adhesion force, μ the static coefficient of friction, and N the normal force.

For the intermediate regime where h is similar to the radius of gyration of the molecules R_g, the rheological behavior still remains unclear, displaying the complex nonlinear feature similar to non-Newtonian fluids [2,17]. In this work, we study this intermediate regime of the interfacial rheology by making new ultrasonic measurements at high amplitude in a sphere-plane contact geometry. The contacts are lubricated by macromolecular films, whose thickness h can be smaller (ultrathin) or larger (thick) than R_g ($\sim$13 nm). We show a mixed nonlinear behavior between the Mindlin-like frictional dynamics as found with small molecules [10,14] and the interfacial adhesive failure, i.e., a bond rupture at highest oscillatory driving [2,8].

In addition, we investigate the steady-state rheological response of these interfacial films by means of sliding experiments, perturbed by the presence of high-amplitude ultrasonic vibration. Here the interfacial sliding is initiated under gravity with an inclined plane. At slow velocity the dissipation is dominated by the pinning of adhesive bridges across a shear band, while at higher velocity viscous damping dominates. When sliding occurs close to the shear threshold σ_0, the controlled ultrasonic perturbation (or pumping) may enhance the sliding velocity by a factor of 2–4. We discuss a mechanism based on the rupture of chain ends at the interfacial bridges.

II. EXPERIMENTS

The experimental setup is represented in Fig. 1(a). First, a thin film of polyisobutylene (PIB, molecular weight

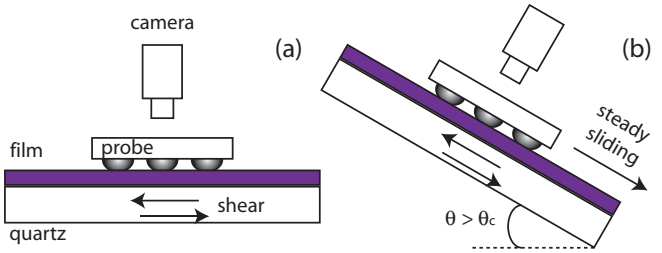

FIG. 1. (Color online) Experimental setup (not to scale). (a) The probe is composed of three lenses stuck on a glass plate and is deposited on a quartz coated with the polymer film. The contact area is viewed with a video camera, while the oscillation amplitude is varied. (b) The apparatus is mounted on a plane which is inclined above the threshold angle θ_c. The movement of the probe during the steady sliding is followed with the same video system as in (a).

$M = 1700$ kg/mol, Akros Organics) is spin coated on a quartz resonator (Inficon) with a resonance frequency $f \sim 5$ MHz (corresponding to a wavelength $\lambda = 600$ μm) from a toluene solution at 0.1%. The quartz is mounted in the measurement cell and is connected to a network analyzer for measuring both the shear resonance frequency f and the quality factor Q of the quartz. The negative frequency shift due to the deposition of the film, of order of magnitude $\Delta f \sim 10^2$ Hz for the systems studied here, provides a measurement of the thicknesses [18], being $h = 10$ to 300 nm. The quality factor was not modified by the deposition of the films.

The probe consists of three BK7 lenses (Melles Griot) attached to a glass plate. After immersion in a solution of sulfuric acid and H_2O_2 (70/30), drying under argon and 10 min of oxygen plasma, the probe is placed for 1 h in a 1% solution of silanes in toluene, providing a low-energy surface. The probe is then placed at the center of the quartz and the radius of contact a ($\sim$10–20 μm) is monitored by means of a video camera imaging through the lenses [Fig. 1(a)].

After establishing the contact between the probe and the quartz, the resonance frequency shifts upwards of Δf, which is proportional to the interfacial stiffness k_T for the long wavelength considered here $\lambda \gg a$ [19–22],

$$\Delta f \sim N_b k_T/(MK)^{1/2}, \tag{1}$$

where $K = 3.0 \times 10^{10}$ N/m and $M = 3 \times 10^{-5}$ kg are the stiffness and the mass of the quartz and N_b is the number of beads effectively covering the quartz electrode. The inverse quality factor shifts of ΔQ^{-1}, proportionally to the dissipated energy per unit energy stored,

$$\Delta Q^{-1} = \frac{1}{2\pi}\frac{\Delta W_d}{\Delta W_e}, \tag{2}$$

where ΔW_d is the energy dissipated, viscous, or/and frictional [23] and $\Delta W_e = K U_T^2$ is the energy stored by cycle.

Two different sets of rheological measurements are realized: oscillatory and steady sliding. In the first [Fig. 1(a)], the shear oscillation amplitude is varied from $U_T \sim 0.01$ to 40 nm [24] without applying any static shear. The frequency shift and the quality factor are measured together with the contact area in order to observe precisely the local behavior of the contacts.

In the second set of measurements, we investigate the sliding behavior when the system is inclined [Fig. 1(b)]. The probe starts to slide at $\theta \geqslant \theta_c$, where θ_c is the angle of repose. The images of the contact recorded during sliding provide the contact area, and the sliding velocity of the probe is measured by tracking position of the contact line as a function of time. The dependence of the sliding velocity V on the shear stress $\sigma = mg \sin\theta/\pi a^2$ (m is the mass of the probe) is obtained by varying θ incrementally with $2.5^\circ < \theta < 11.5^\circ$. For each combination of (θ, U_T), the movement of the probe is followed during at least 60 s, which ensures that a steady sliding regime is reached, as checked *a posteriori* from spatiotemporal diagrams achieved with IMAGEJ software.

To study the effects of high-amplitude ultrasonic vibrations on the sliding, we apply the protocol sketched in the inset of Fig. 5. With the plane inclined at $\theta \geqslant \theta_c$, the probe slides at a velocity V_i while a nonperturbative ultrasound $U_T \sim 0.1$ nm is applied to monitor the interfacial film. Then the ultrasonic amplitude is set to a higher value U_{Ti}, leading to a higher sliding velocity $V^{vib}(U_{Ti})$. After applying such perturbative high-amplitude vibrations, reference measurements of V_i at $U_T \sim 0.1$ nm are taken again. The reference sliding velocity V is computed from the average of the V_is for a given θ. This ensures that changes of the sliding velocity by high-amplitude vibrations are not blurred by sporadic irregularities of the spin-coated film.

III. RESULTS

A. Oscillatory response of ultrathin films

Figure 2 shows four different regimes under ultrasonic shear oscillation in the absence of static shear loading. When the amplitude of the vibration is small, in regime 1 (linear), the frequency shift and the inverse of the quality factor are constant. One measures experimentally a contact area of radius $a \approx 20$ μm as shown in Fig. 3 (left panel on the top).

In regime 2, the frequency shift (or the stiffness) decreases while the inverse of quality factor increases. The behavior of this regime seems similar to what is expected with a frictional interface [13,14]. Regime 3 corresponds to a range of oscillation amplitudes where the inverse of the quality factor decreases while the frequency shift continues to decrease but with a different slope from regime 2.

Regime 4 corresponds to the response probed in this work at highest amplitude, $U_T \sim$ 20–50 nm. We observe a dramatic change of the morphology of the contact as shown in Fig. 3. When the amplitude exceeds 17 nm, the contact radius defined by the dark zone in Fig. 3 decreases continuously and reaches 50% of its initial value at $U_T \sim 45$ nm, which is close to the Hertzian contact radius $a_H \sim 10$ μm without the thin film. Some pattern, similar to droplets left after dewetting, forms. A small-amplitude measurement shows that the interfacial stiffness k_T is here reduced nearly by a factor 2 compared to the initial linear stiffness.

Regarding the sliding experiment of these ultrathin films, the probe remains stuck at $\theta < \theta_c$ and accelerates abruptly when the plane is inclined to $\theta = \theta_c$. Therefore, it is impossible to achieve a steady sliding with this system within the field of view of the camera. However, high-amplitude ultrasonic

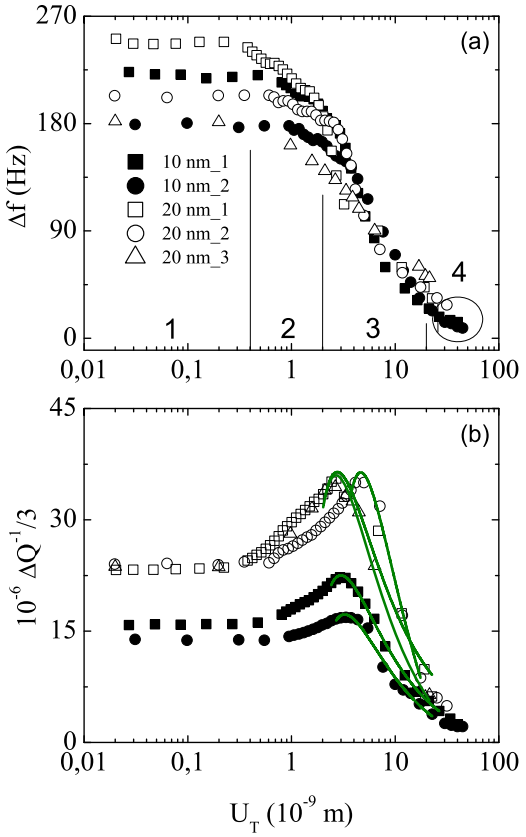

FIG. 2. (Color online) Shift of resonance frequency (a) and inverse of quality factor (b) as a function of the amplitude of oscillation for two polyisobutylene films. Black and white symbols represent several measurements for thicknesses 10 and 20 nm, respectively. Green (light gray) lines are fit to Eq. (9) (see text). When the amplitude of oscillation varies, four distinct regimes can be identified. See Fig. 1(a), $\theta = 0$.

vibrations have a dramatic effect on the static threshold, similar to systems with small molecules [10].

B. Steady sliding of thick films

The rheological behavior of thicker films of $h \geqslant 50$ nm is quite different. The oscillatory response at $\theta = 0$ is basically linear, corresponding to regime 1. For the whole range of

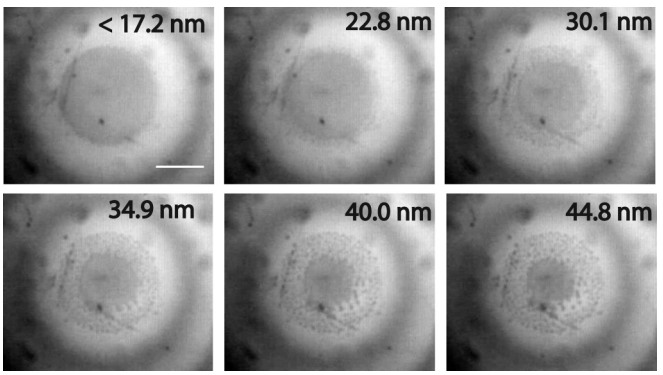

FIG. 3. Images of the contact area under oscillations. The amplitude of oscillation is indicated on each image. $h = 10$ nm; $\theta = 0$.

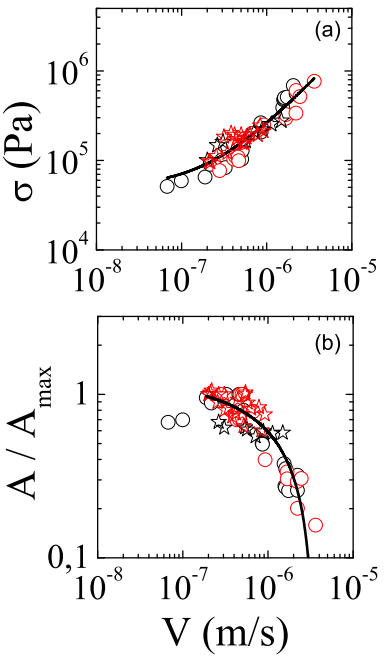

FIG. 4. (Color online) (a) Shear stress as a function of sliding velocity. The solid line is a fit of experimental data with $\sigma = \sigma_0 + kV$. (b) Contact area as a function of the velocity. Spheres and stars correspond to polymer films of 50 and 300 nm. The solid line is a fit with Eq. (12). Black symbols and red (light gray) symbols are data without and with vibrations, respectively.

amplitude achievable with the present setup, the area of contact is constant whatever the oscillation amplitude. As far as the steady sliding is concerned when $\theta \gtrsim \theta_c$, the probe moves slowly at 0.1 μm/s, as shown in Fig. 4(a). The data obtained without ultrasonic vibrations roughly follow an empirical relationship,

$$\sigma = \sigma_0 + \kappa V, \tag{3}$$

where $\sigma_0 = 30$ kPa is the sliding threshold and $\kappa = 10^{11}$ Pa s m^{-1}. The area of contact $A = \pi a^2$ decreases with the sliding velocity, as shown Fig. 4(b). The effect of the vibrations on the steady state sliding velocity is shown Fig. 5 at $\theta \geqslant \theta_c$ for films of 50 and 300 nm. Oscillation amplitudes lower than 0.1 nm have no effect. For U_T larger than a threshold $U_c \sim 1$ nm, the velocity increases progressively until a factor of 4 for $U_T \sim 10$ nm. The application of shear vibrations does not, however, change the value of κ within the precision of the measurement [Fig. 4(a)].

IV. DISCUSSION

A. Frictional dynamics in ultrathin films

For the intermediate regime considered here ($h \sim 10$ nm) and in the absence of static shear, the contact zone of radius $a \sim 20$ μm between the sphere and the quartz may be viewed as a Hertzian-like solid contact at the center of radius $a_H \sim 10$ μm with a PIB film squeezed at the edge, i.e., kind of rim. The shear stiffness of this inhomogeneous interface k_T may thus be considered approximately as the addition of the contact stiffness k_M (Mindlin-like) and the film stiffness k_{rim} (rim).

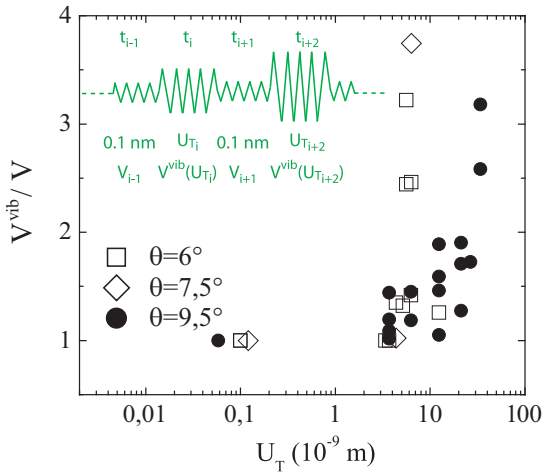

FIG. 5. (Color online) Sliding velocity under vibrations V^{vib} normalized by the sliding velocity without vibrations, versus oscillation amplitude. The film thickness is 50 nm for white symbols) and 300 nm for black symbols. The inset details the protocol used for the measurements (see text).

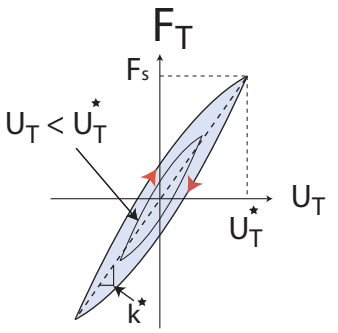

FIG. 6. (Color online) Hysteresis cycle for oscillation amplitudes corresponding to a shear force inferior, and equal, to the threshold friction force F_s [16].

1. *Growth of the microslip annulus*

The responses observed in regimes 1 and 2 (Fig. 2) are very similar to those previously found on the interface with small molecules. In regime 1 (linear regime), the interfacial shear stiffness and dissipation are dominated by the viscoelastic properties of the thin film and by those of the contacting solids (spheres and quartz), even though they are difficult to be determined quantitatively due to the heterogeneity and the geometry of the film.

In regime 2, the nonlinear behavior of the stiffness softening and the amplitude-dependent dissipation can be qualitatively explained by a Mindlin-like friction model, involving the micro (partial) slip within the solid contact [10,14]. When the oscillation amplitude U_T is larger than a critical value U_c, a microslip annulus grows at the periphery of the contact. In this case, the interfacial stiffness shall decrease with the oscillatory force F_T (the film stiffness k_{rim} is assumed to be constant and is neglected in the following analysis for simplicity [25]), such that [26]

$$k_T \sim k_M\left(1-\frac{F_T}{6\mu N}\right), \tag{4}$$

where μ is the static coefficient of friction, N the normal load, and k_M the linear shear stiffness. The frictional dissipation per cycle corresponds to the hysteresis loop represented in Fig. 6, being proportional to the cube of the oscillating force at relatively low amplitude [27],

$$\Delta W_d = F_T^3/36a_H\mu N G^*, \tag{5}$$

with G^* the effective modulus of the contacting solids.

Assuming $F_T \sim k_T U_T$, measurements of the frequency shift and the inverse quality factor provide two independent ways for estimating the friction coefficient μ. In Fig. 7(a), we replot k_T/k_M from Fig. 2 as a function of F_T, resulting in linear curves with slope $\mu \sim 0.4 \pm 0.1$. In Fig. 7(b), normalized ΔQ^{-1} such that $B\frac{\Delta Q^{-1}}{k^3(U_T)} = \mu U_T$ are also replotted with constant $B = 36\pi a_H K N G^*$. Again, the curves are linear, giving $\mu \sim 0.14 \pm 0.05$. The difference between the two estimates may arise from fluctuations caused by a small surface area associated with the sliding annulus [28] and cumulated errors from estimated material parameters. Nevertheless, the order of magnitude obtained from elastic and dissipative parts of the oscillatory response is consistent, supporting conveniently the scenario of the partial microslip in regime 2. Note that the initial growth of the microslip annulus can be

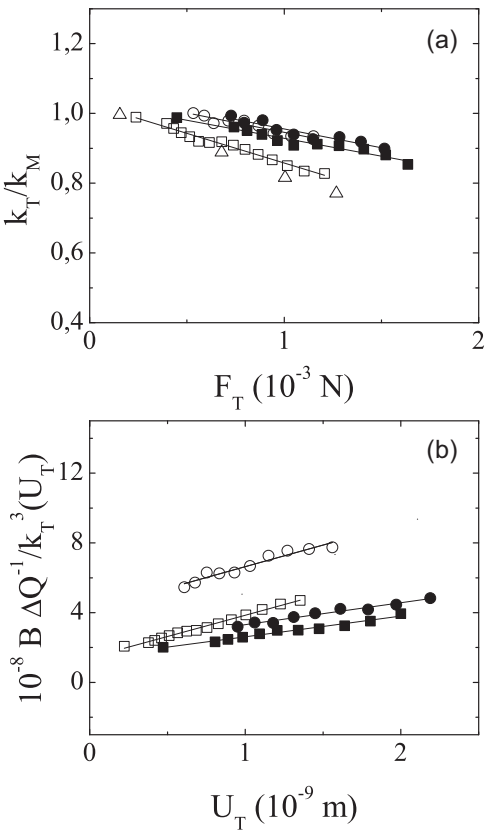

FIG. 7. Microslip regime 2. (a) k_T/k_M as a function of F_T. Straight lines are fits to Eq. 4 (b) Normalized quality factor as a function of the oscillation amplitude U_T. According to the text, the slope equals the coefficient of friction. $\theta = 0$.

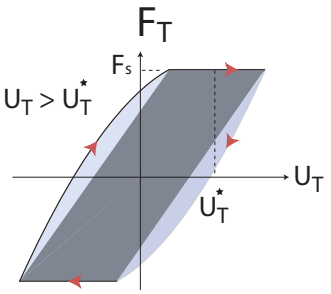

FIG. 8. (Color online) Proposed hysteresis cycle for oscillation amplitudes corresponding to full slip. The Mindlin cycle corresponds to light gray. Dissipation due to full slip is represented in dark gray.

alternatively described as an opening crack at the edge of the contact [29].

2. *Beyond the full slip*

In regime 3 (Fig. 2), the frequency shift continues to decrease but the inverse of the quality factor decreases as well. Such a maximum in ΔQ^{-1} indicates a transition from partial microslip to full slip, during which the dynamic behavior of the contact alternates between a Mindlin frictional regime and a full slip regime, characterized by the dynamic coefficient of friction as sketched in Fig. 8. A similar regime has been studied recently in [30,31]. The dissipation depends on two components. One of them is constant and is the maximum area of a Mindlin cycle [27] (Fig. 6),

$$\Delta W_d^\star = \frac{3}{20}\frac{(\mu N)^2}{a_H G^*}, \tag{6}$$

where $\mu N = F_s = k^\star U_T^\star$, $k^\star$ is the secant stiffness at the threshold, and $U_T^\star$ is the corresponding oscillation amplitude. The second one results from full slip once the friction threshold is reached and can be estimated from the proposed simple hysteresis cycle as shown in Fig. 8,

$$\Delta W_s = 4F_s\left(U_T - U_T^\star\right). \tag{7}$$

The total dissipation is

$$\Delta W = \Delta W_d^\star + \Delta W_s. \tag{8}$$

The inverse of the quality factor measured includes the two terms $\Delta Q^{-1\star} = \frac{1}{2\pi}\frac{\Delta W^\star}{1/2KU_T^{\star 2}}$ and $\Delta Q_s^{-1} = \frac{1}{2\pi}\frac{\Delta W_s}{1/2KU_T^2}$ and results in, after rearrangement,

$$\Delta Q^{-1} = \frac{1}{2\pi}\left[\frac{3k^{\star 2}}{10Ka_H G^*} + \frac{8F_s(U_T - U_T^\star)}{KU_T^2}\right]. \tag{9}$$

Fitting experimental data shown in Fig. 2(b) provides an estimate for the dynamic friction force $F_s \approx 5 \pm 3$ mN and for the threshold amplitude for full slip $U_T^\star \approx 1.6 \pm 0.4$ nm.

For the model to be valid, the value of F_s obtained from the measurement of the dissipation shall correspond to $F_T = k_T U_T = F_s$ in regime 3, which is a constant. This is shown in Fig. 9, where $F_s \approx 3$ mN is close to the estimate from the dissipation data. Therefore, the postulated hysteresis cycle in Fig. 8 is consistent with the two independent measurements for the elasticity and the dissipation. After reaching the threshold force the system alternates between microslip as described by Mindlin and periodic full slip at ultrasonic frequency.

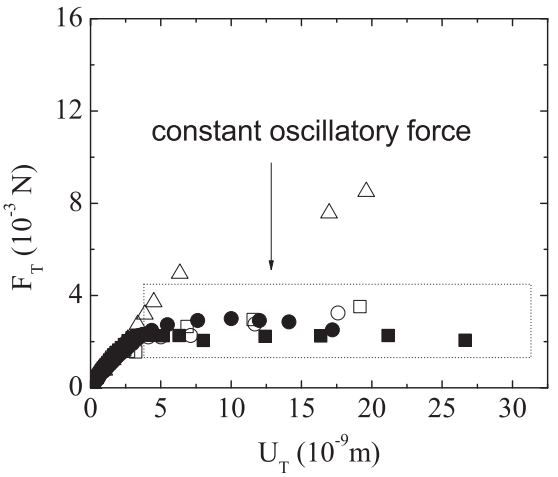

FIG. 9. Oscillatory shear force $F_T = k_T U_T$ as a function of U_T. For large shear amplitudes U_T the shear force is constant. The legend is the same as Fig. 2. $\theta = 0$.

3. *Chain rupture*

Observed at the highest amplitudes, regime 4 corresponds to a situation where the frequency shift, or the stiffness k_T, almost vanishes, implying the decrease of k_{rim}. While the high-oscillating shear causes failure, the interfacial layer detaches, as shown in Fig. 3, corresponding to a reduction of the contact area by a peelinglike mode with a slight normal separation between the contacting surfaces [8]. The oscillatory energy necessary for decreasing the contact surface area (see Fig. 3) from the contact radius a to the actual contact radius a_r under the highest amplitude of oscillations is

$$E_r \sim \tfrac{1}{2}k_T U_T^2 \sim \Gamma\epsilon^2, \tag{10}$$

where Γ is the energy necessary for debonding a unit area of adhesive contact and $\epsilon^2 = \pi(a^2 - a_r^2)$.

The plots of the oscillatory energy versus the decreased contact area are roughly linear, as shown in Fig. 10, giving $\Gamma \approx 30\ \mathrm{mJ\,m^{-2}}$.

At ultrasonic frequencies and room temperature, polyisobutylene is nearly glassy [32] and the failure shall be brittle. For a molecular bond rupture $E_b \sim 1$ eV, and assuming that every entanglement strand of length $\xi \sim 2$ nm [33] is broken, one obtains the energy of rupture $E_r \sim E_b/\xi^2 \sim 40\ \mathrm{mJ/m^2}$, equivalent to Γ as estimated from experimental data.

The present observations may connect naturally to recent studies where the onset of motion of multicontact interfaces is analyzed in terms of the propagation of rupture fronts [8] initiated at the edge of the slider. The perturbation by highest amplitude oscillations $2 < U_T < 100$ μm at $0.1 < f < 500$ Hz modifies the stick-slip dynamics by altering the slow rupture modes. Our results suggest that regimes 1 to 3 discussed here may precede rupture fronts, as observed in regime 4, and shall be taken into account for a complete description of the sliding threshold.

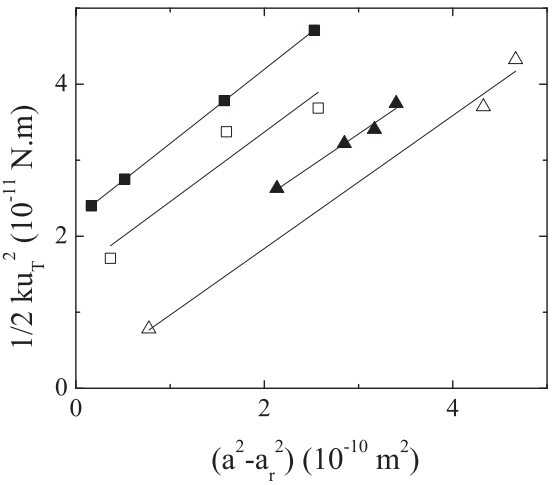

FIG. 10. Decrease of surface area plotted against oscillatory energy. $\theta = 0$.

B. Steady sliding under vibrations in thick films

1. Viscous losses and lift

At high sliding velocity, the shear stress at the polymer-solid interface can be written $\sigma_s = \kappa V$ [34], where κ is a constant depending on the viscosity and the thickness sheared, and V is the steady sliding velocity. As discussed in [34], for long macromolecules the slip length is of the order of hundreds of microns, much larger than the thickness of the thin films, and no bulk dissipation shall take place. All viscous losses are localized in a slip plane (or shear band) of thickness D such that $\kappa = \frac{\eta_e}{D}$. Here $\eta_e = N_e\eta_0$, where η_0 is the viscosity of the monomer fluid and $N_e \sim 20$ the number of segments between entanglements. With $\eta_0 \sim \zeta_0/b$ ($\zeta_0 = 4.5 \times 10^{-8}$ N s m^{-1} [32], $b \sim 1$ nm), $\kappa \sim \zeta_0 N_e^{1/2}/b^2 \sim 10^{11}$ Pa s m^{-1}, as found experimentally in the present study [Fig. 4(a)].

The shear flow inside the shear band can be described in the hydrodynamic lubrication approximation by

$$\eta_e \frac{\partial^2 V}{\partial y^2} = \frac{\partial P}{\partial x}, \tag{11}$$

which scales as $\eta_e V/D^2 \sim P/a$ and gives $D \sim (\frac{\eta_e V a}{P})^{1/2}$ (P is the pressure). Combined with the geometrical relation $a^2 \sim 2(h - D)R$, where R is the radius of the spherical probe, this leads to

$$\frac{A}{A_{max}} \sim 1 - \left(\frac{\eta_e a}{P h^2}\right)^{1/2} V^{1/2}. \tag{12}$$

Due to the shear flow, the probe lifts, which results in a decrease of the contact area. Fitting experimental data in Fig. 4(b) with Eq. (12) provides a prefactor $(\frac{\eta_e a}{P h^2})^{1/2} = 680 \pm 50$ $(s/m)^{1/2}$ consistent with expected value $\sim 10^3$, obtained with $mg \sim 3.6 \times 10^{-3}$ kg, $\eta_e \sim 1000$ Pa s, $a \sim 10$ μm, and $h \sim 10$ nm. This gives a reasonable agreement with the scaling, considering the simplification made on the flow profile (three-dimensional effects for the sphere-plane geometry) and the approximation on the contact radius (the conservation of volume has to be taken into account).

2. The threshold: Rupture and diffusion of interfacial bridges [35]

At low sliding velocity, viscous dissipation such as that discussed above vanishes. Instead, dissipation arises from ruptures of chain ends entangled at the interface.

The dynamics of the polymer chains located at the interface between an elastomer and a solid surface are heterogeneous. Some chains with low mobility stick on the solid surface because of segmental adsorptions. The chains away from the surface have higher mobility but interact with stuck chains by forming interfacial bridges *via* entanglements formed by diffusion of chain ends. These bridges constitute a weak interface and are created when the Rouse modes of N_e segments diffuse across the shear band. This process is characterized by a normal velocity $V^* \sim D/\tau_R$, with $\tau_R \sim \tau_0 N_e^2$, where $\tau_0 \sim \zeta_0 b^2/k_b T$ is the diffusion time of the monomers. During stationary sliding, the creation by diffusion is, however, in competition with the destruction by shear at the velocity of sliding V. Then, a rate equation for the dependence of the density of bridges on the steady sliding velocity writes

$$\nu = \frac{\nu_0}{1 + V/V^*}, \tag{13}$$

where $\nu_0 \sim 1/(b^2 N^{1/2})$ is the maximum surface density of bridges [35] and $N \sim 1000$.

When the shear velocity $V \gg V^*$, no bridge can form ($\nu = 0$) and the shear stress is only dependant on the viscous dissipation of the shear band described by κ. For the system considered here, $\tau_R \sim 10^{-3}$ s and $V^* \sim 1$ μm s^{-1}. This is indeed the range of velocity where the viscous term becomes dominant in our experiments as shown in Fig. 4(a).

When V vanishes, $\nu = \nu_0$ defines the shear threshold stress $\sigma_0 = \nu_0 f_b$, where $f_b \sim k_b T/b N_e^{1/2}$ (k_b is the Boltzmann constant) is an order of magnitude for the rupture force of a single bridge. For the polyisobutylene used in this work, $\sigma_0 \sim 10$ kPa, which is similar to the extrapolation of our experimental data to zero velocity [Fig. 4(a)], as given by the empirical fit $\sigma = \sigma_0 + \kappa V$.

3. Steady sliding under ultrasonic oscillations

As pointed out in [2], the effect of vibrations on the steady state rheological response depends on both frequency and amplitude. The above description suggests that in the present study the interfacial dynamics is governed by a single characteristic time τ_R, which is necessary for the interfacial bridge to heal from a possibly vibration-induced breaking if the condition $\omega\tau_R < 1$ is verified. However, at ultrasonic frequencies, the condition $\omega\tau_R \gg 1$ is always fulfilled. Hence, U_T is the principal parameter of control for an efficient perturbation of the interfacial dynamics. As done earlier for ultrathin films, we estimate the surface vibrational energy input during sliding $\sim \frac{1}{2} \times k U_T^2/\pi a^2$. With $U_T \sim 10$ nm, $a \sim 20$ μm, $k \sim 10^6$ N m^{-1}, the surface energy above which the velocity of sliding is affected amounts to ~ 40 mJ m^{-2}, which corresponds to the energy of chain scission discussed for the ultrathin films.

Finally, when the sliding velocity is close to the threshold as considered here, dissipation arises mainly from the adhesive part of the shear stress σ_0. We may estimate a relative increase of the sliding velocity at a given stress (or inclination angle

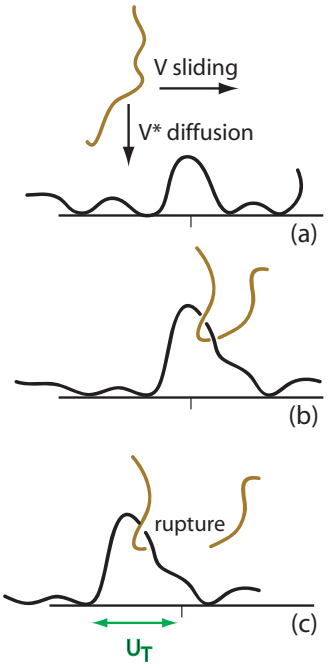

FIG. 11. (Color online) (a) The chain diffuses during sliding and (b) entangles with chains adsorbed on the surface. (c) Vibrations rupture entangled chains.

θ) by $\frac{\Delta V}{V} = \frac{\sigma_0}{kV}$ if σ_0 is reduced to zero by high-amplitude shear vibration [10]. Such increase would be $\sim$100% at $V \sim 0.1\ \mu\mathrm{m\,s}^{-1}$, qualitatively explaining the increase of sliding velocity observed in Fig. 5. A possible scenario is proposed in Fig. 11, showing that vibrations may affect the interaction of chain segments with the surface. Namely, oscillations shall rupture interfacial bridges, affecting the state variable ν and resulting in an increase of the sliding velocity.

V. CONCLUSION

To sum up, we have investigated the rheological behavior of thin macromolecular films by both oscillatory ultrasonic and stationary sliding measurements. Our main results are (i) when no static shear stress is applied, increasing oscillation amplitude gives rise to, respectively, linear, microslip, full slip, and peelinglike rupture regimes; (ii) during a steady sliding state close to the threshold σ_0, application of ultrasonic shear vibrations increase the velocity of sliding. This latter is presumably due to the perturbation of the adhesive term σ_0 by rupture of chain ends. The extent to which the nonlinear vibrations modify the effective viscosity (κ) needs to be further investigated, for example, with a configuration in which the driving velocity is controlled [7,8].

This study may also help to better understand the effect of nonlinear vibration on the yield-stress rheology of amorphous systems such as granular materials. Indeed, a breakdown of local shear elasticity due to vibrations may have dramatic consequences on the cohesion of granular media by initiating multiple fractures or rearrangements, leading to global collapse such as avalanche or landslide.

ACKNOWLEDGMENTS

We wish to acknowledge Hubert Sizun (LPMDI) for his help in the realization of the experimental setup and Institut Carnot VITRES for financial support.

[1] B. N. J. Persson, *Sliding Friction: Physical Principles and Applications* (Springer, Berlin, 1998).
[2] M. Heuberger, C. Drummond, and J. N. Israelachvili, J. Chem. Phys. **102**, 5038 (1998).
[3] J. Krim, Adv. Phys. **61**, 155 (2012).
[4] J. B. Sokoloff, J. Krim, and A. Widom, Phys. Rev. B **48**, 9134 (1993).
[5] K. Dahmen and J. P. Sethna, Phys. Rev. B **53**, 14872 (1996).
[6] J. F. Joanny and P. G. de Gennes, J. Chem. Phys. **81**, 552 (1984).
[7] L. Bureau, C. Caroli, and T. Baumberger, Proc. R. Soc. London, Ser. A **459**, 2787 (2003).
[8] R. Capozza, S. M. Rubinstein, I. Barel, M. Urbakh, and J. Fineberg, Phys. Rev. Lett. **107**, 024301 (2011).
[9] P. Johnson, H. Savage, M. Knuth, J. Gomberg, and C. Marone, Nature (London) **451**, 57 (2008).
[10] J. Léopoldès, G. Conrad, and X. Jia, Phys. Rev. Lett **110**, 248301 (2013).
[11] K. Dalnoki-Veress, B. G. Nickel, C. Roth, and J. R. Dutcher, Phys. Rev. E **59**, 2153 (1999).
[12] L. Léger and C. Creton, Philos. Trans. R. Soc., A **366**, 1425 (2008).
[13] S. Berg and D. Johannsmann, Phys. Rev. Lett. **91**, 145505 (2003).
[14] J. Léopoldès and X. Jia, Phys. Rev. Lett. **105**, 266101 (2010).
[15] M. Ruths and J. N. Israelachvili, in *Handbook of Nanotechnology*, edited by D. Bushnan (Springer, Berlin, 2007), pp. 859–924.
[16] R. D. Mindlin, ASME Trans. J. Appl. Mech. **16**, 259 (1949).
[17] A. L. Demirel and S. Granick, Phys. Rev. Lett. **77**, 2261 (1996).
[18] G. Sauerbrey, Z. Phys. **155**, 206 (1959).
[19] G. L. Dybwad, J. Appl. Phys. **58**, 2789 (1985).
[20] D. Johannsmann, New J. Phys. **10**, 053014 (2008).
[21] J. Léopoldès and X. Jia, Europhys. Lett. **88**, 34001 (2009).
[22] A. Laschitsch and D. Johannsmann, J. Appl. Phys. **85**, 3759 (1999).
[23] T. Brunet, X. Jia, and P. Mills, Phys. Rev. Lett. **101**, 138001 (2008).
[24] B. A. Martin and H. E. Hager, J. Appl. Phys. **65**, 2630 (1989).
[25] If $k_{rim} \approx k_M$ is accounted for in Eq. (4), $k_T \approx k_{rim} + k_M(1 - \frac{F_T}{6\mu N})$, then the friction coefficient μ fitted from Fig. 7(a) would be smaller by a factor of about two.
[26] X. Jia, Th. Brunet, and J. Laurent, Phys. Rev. E **84**, 020301(R) (2011).
[27] K. L. Johnson, *Contact Mechanics* (Cambridge University Press, Cambridge, UK, 1985).

[28] T. Baumberger and C. Caroli, Adv. Phys. **55**, 279 (2006).
[29] A. R. Savkoor and G. A. D. Briggs, Proc. R. Soc. London, Ser. A **356**, 103 (1977).
[30] B. Borovsky, A. Booth, and E. Manlove, Appl. Phys. Lett. **91**, 114101 (2007).
[31] S. Hanke, J. Petri, and D. Johannsmann, Phys. Rev. E **88**, 032408 (2013).
[32] J. D. Ferry, *Viscoelastic Properties of Polymers* (Wiley, New York, 1980).
[33] M. Rubinstein and R. H. Colby, *Polymer Physics* (Oxford University Press, Oxford, UK, 2003).
[34] F. Brochard-Wyart, C. Gay, and P. G. de Gennes, Macromolecules **29**, 377 (1996).
[35] F. Brochard-Wyart and P. G. de Gennes, Eur. Phys. J. E **23**, 439 (2007).